Applied Physics Letters

Robust frame-reduced structured illumination microscopy with accelerated correlation-enabled parameter estimation Ⓕ

ⓈⒸⒾ

ⓘⅅ Jiaming Qian, Yu Cao, ⓘⅅ Kailong Xu, et al.

COLLECTIONS

Note: This paper is part of the APL Special Collection on Advances in Optical Microscopy for Bioimaging.

Ⓕ   This paper was selected as Featured

ⓈⒸⒾ   This paper was selected as Scilight

View Online   Export Citation   CrossMark

AIP Publishing

Robust frame-reduced structured illumination microscopy with accelerated correlation-enabled parameter estimation
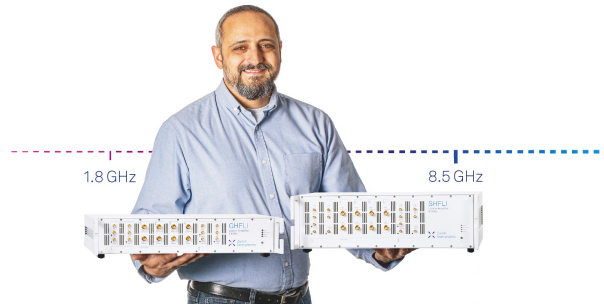
View Online   Export Citation   CrossMark

Jiaming Qian,[1,2,3,a] (iD) Yu Cao,[1,2,3] Kailong Xu,[1,2,3] (iD) Ying Bi,[1,2,3] Weiyi Xia,[1,2,3] Qian Chen,[3] (iD) and Chao Zuo[1,2,3,b] (iD)

AFFILIATIONS

[1]Smart Computational Imaging (SCI) Laboratory, Nanjing University of Science and Technology, Nanjing, Jiangsu Province 210094, China
[2]Smart Computational Imaging Research Institute (SCIRI) of Nanjing University of Science and Technology, Nanjing, Jiangsu Province 210019, China
[3]Jiangsu Key Laboratory of Spectral Imaging & Intelligent Sense, Nanjing, Jiangsu Province 210094, China

Note: This paper is part of the APL Special Collection on Advances in Optical Microscopy for Bioimaging.
[a]Electronic mail: jiaming_qian@njust.edu.cn
[b]Author to whom correspondence should be addressed: zuochao@njust.edu.cn

ABSTRACT

Structured illumination microscopy (SIM), with the advantages of full-field imaging and low photo-damage, is one of the most well-established fluorescence super-resolution microscopy techniques that raised great interest in biological sciences. However, conventional SIM techniques generally require at least nine images for image reconstruction, and the quality of super-resolution significantly depends on high-accuracy illumination parameter estimation, which is usually computationally intense and time-consuming. To address these issues, we propose a robust seven-frame SIM reconstruction algorithm with accelerated correlation-enabled parameter estimation. First, a modulation-assigned spatial filter is employed to remove unreliable backgrounds associated with low signal-to-noise ratios. Then, we propose a coarse-to-fine accelerated correlation algorithm to eliminate the redundant iterations of the traditional correlation-based scheme. The frame reduction is achieved by a specially designed phase-shifting strategy combined with pixel-wise fluorescence pre-calibration. We experimentally demonstrate that, compared with conventional iterative correlation-based methods, the proposed algorithm improves the computational efficiency by a factor of 4.5 while maintaining high accuracy illumination parameter estimation. Meanwhile, our method achieves high-quality super-resolution reconstruction even with a reduction in two raw images, which improves the efficiency of image acquisition and ensures the robustness toward complex experimental environments.

Published under an exclusive license by AIP Publishing. https://doi.org/10.1063/5.0107510

As an essential tool for biological research, optical microscopes help mankind gain insight into the microworld with its nondestructive and flexible advantages. Classical optical microscopy, however, limited by the Abbe diffraction limit ($\sim$200 nm), fails to observe nanoscale subcellular features.[1] In the past decades, a series of fluorescence super-resolution microscopy techniques have been explored to break the diffraction barrier, mainly including photoactivated localization microscopy (PALM),[2] stochastic optical reconstruction microscopy (STORM),[3] stimulated emission depletion (STED) microscopy,[4] and structured illumination microscopy (SIM).[5–7] Among them, SIM, with the advantages of fast full-field imaging and low photo-damage, is especially suitable for the study of live cells.[8,9]

SIM achieves a twofold expansion of the lateral resolution by modulating the sample information over the cutoff frequency into the detection passband through structured illumination. Therefore, the necessary demodulation/reconstruction algorithms are critical to ensure the quality of super-resolution.[10,11] Typically, nine raw structured illumination images are required for each SIM reconstruction, which, despite the higher temporal resolution compared with other super-resolution techniques such as PALM or STORM requiring thousands of exposures, still struggles to meet the demands of live-cell observation. Another frequent criticism of SIM is image artifacts caused by inaccurate estimation. That is because the reconstruction algorithm of SIM extremely depends on the illumination parameters,

which are usually post-estimated from the raw SIM data. On the one hand, to reduce the number of raw frames of SIM data and improve the image acquisition speed/imaging efficiency (which would bring additional benefits of lower phototoxicity and photobleaching), some frame-reduction space domain iterative algorithms are proposed.[12–14] However, these methods require some *a priori* assumptions about illumination patterns and they are often vulnerable to noise. A frequency domain SIM algorithm for frame reduction has also been proposed, but it is time-consuming and the reconstruction image is affected by artifacts.[15] In addition, deep learning has also been applied to frame-reduction SIM reconstruction, but its "black-box" nature makes it difficult to ensure reliable and stable results.[16–18] Therefore, the conventional nine-frame approach based on phase-shifted spectrum separation is still preferred for imaging fidelity and adaptability to the practical environment.[19,20] On the other hand, several fast parameter estimation algorithms have been proposed for the knowledge of illumination parameters (wave vector, initial phase, and modulation depth), but their accuracy is compromised for speed and the robustness is susceptible to low signal-to-noise ratio (SNR).[21–23] The iterative correlation-based (COR) approach is probably the most widely available parameter estimation technique, which ensures better accuracy and noise immunity through sub-pixel optimization in the form of real-space phase gradients.[24,25] However, the iterative optimization is time-consuming, further reducing the imaging efficiency of SIM.

To address these problems, simultaneously ensuring practicality and robustness, we consider optimizing conventional parameter estimation and image reconstruction methods to improve the efficiency of super-resolution reconstruction. With coarse-to-fine accelerated correlation-enabled parameter estimation and frame-reduced image reconstruction combined with pixel-wise fluorescence pre-calibration, high-quality super-resolution images can be obtained from only seven raw SIM images preprocessed by the modulation-assigned spatial filter in complex experimental environments.

In conventional SIM, three-step phase-shifting sinusoidal structured illumination patterns of three directions (totally nine frames) are required to achieve isotropic super-resolution, each of which can be expressed as

$$D_{n,j}(\mathbf{r}) = \left\{ S(\mathbf{r}) \left[1 + m_n \cos\left(2\pi \mathbf{p}_n \mathbf{r} + \varphi_{n,j} + \varphi_n^0\right) \right] \right\} \odot H(\mathbf{r}), \quad (1)$$

where $\mathbf{r}$ represents the spatial coordinates; $\odot$ is the convolution operation; the subscripts n ($n = 1, 2, 3$) and j ($j = 1, 2, 3$) denote the nth direction and the jth phase shift, respectively; S is the sample information; H is the point spread function (PSF) of the microscopy; φ represents the phase shift; and $\mathbf{p}$, φ^0, and m are the wave vector, initial phase, and modulation of the illumination pattern, respectively. Its Fourier spectrum can be expressed as

$$\tilde{D}_{n,j}(\mathbf{k}) = \left\{ \tilde{S}_0(\mathbf{k}) + \frac{m_n}{2} \exp\left[i(\varphi_n^0 + \varphi_{n,j}) \right] \tilde{S}_{+1}(\mathbf{k} - \mathbf{p}_n) \right.$$
$$\left. + \frac{m_n}{2} \exp\left[-i(\varphi_n^0 + \varphi_{n,j}) \right] \tilde{S}_{-1}(\mathbf{k} + \mathbf{p}_n) \right\} \tilde{H}(\mathbf{k}), \quad (2)$$

where $\mathbf{k}$ represents the frequency coordinate, $\sim$ denotes the Fourier transform of the original object, subscripts 0 and ± 1 are the orders of the separated spectrums, and $\tilde{H}$ represents the optical transfer function (OTF). Through the known phase shift $\varphi_{n,j}$, the 0- and ± 1-

order spectrum components [$\tilde{C}_{n,0} = \tilde{H}(\mathbf{k})\tilde{S}_0(\mathbf{k})$, $\tilde{C}_{n,\pm 1} = m_n \tilde{H}(\mathbf{k})$ $\tilde{S}_{n,\pm 1}(\mathbf{k} \mp \mathbf{p}_n) \exp(\pm i\varphi_n^0)$] can be separated, where ± 1-order spectrums ($\tilde{C}_{n,\pm 1}$) contain high-frequency information of the sample outside OTF. It is not difficult to notice that three zero-order spectrums ($\tilde{C}_{n,0}$) representing the wide-field information among a total of nine separated components in three illumination directions can be shared. Therefore, only seven SIM images are theoretically required to obtain all the effective spectrum components for super-resolution, i.e., seven unknowns can be solved by associating a system of seven linear equations. However, the imperfect system leads to unbalanced fluorescence distribution in different illumination directions, so, in practice, $\tilde{C}_{n,0}$ are not consistent with each other, which will transfer errors to other spectrum components during the joint solution, causing reconstruction artifacts. To address such problems, we propose a robust seven-frame SIM reconstruction algorithm combined with pixel-wise fluorescence pre-calibration, the flow of which is shown in Fig. 1.

In the first illumination direction, conventional three-step phase-shifting illumination mode is adopted for well-separated zero-order spectrum $\tilde{C}_{1,0}$ [Figs. 1(a)–1(c)]. For the other two directions, a pre-calibration scheme can be used to compensate for the above-mentioned imbalance caused by the system. In short, we first individually acquire the wide-field information $C_{n,0}$ (inverse Fourier transform of $\tilde{C}_{n,0}$) for all three directions and then calculate the ratio of the sum of fluorescence intensities in a rectangular box centered at each pixel in $C_{2,0}$ or $C_{3,0}$ for that in $C_{1,0}$ to obtain the calibration parameters (the detailed calibration flow is provided in Note S1 of the supplementary material). It is worth mentioning that the calibration is performed in advance, which is not repeated in subsequent experiments. When the calibration parameters are obtained, $C_{2,0}$ and $C_{3,0}$ can be directly accessed through $C_{1,0}$ [Fig. 1(d)]. The compensated wide-field information is then used to solve for the ± 1-order spectrums in the second and third illumination directions, where two illumination patterns with 0 and $\pi/2$ phase shifts are, respectively, used and those after removing the wide-field components can be represented as [Figs. 1(d) and 1(e)]

$$\tilde{D}_{n,j}(\mathbf{k}) = -i^j \left[\tilde{C}_{n,+1} + (-1)^j \tilde{C}_{n,-1} \right], \quad (3)$$

where $n = 2$ and 3, and $j = 1$ and 2. Then, $\tilde{C}_{2 \, or \, 3, +1}$ and $\tilde{C}_{2 \, or \, 3, -1}$ can be easily solved. Note that once the zero-order components in Eq. (2) are removed, the high-frequency information can theoretically be separated by two illumination patterns with arbitrary phase shifts, where the combination of 0 and $\pi/2$ allows for the least amount of computation and the minimum possible undercompensation-induced error amplification.

Due to the presence of the initial phase, the separated spectrum cannot be reorganized directly for super-resolution reconstruction without image artifacts, which also requires precise knowledge of the wave vector of the illumination. For accurate parameter estimation, COR is preferred to reduce the influence of low SNR on the results, but its expensive computational cost significantly decreases the efficiency of SIM reconstruction. Actually, since it was proposed, COR has hardly been refined for the iterative optimization strategies, especially in terms of speed. Here, we propose a coarse-to-fine accelerated correlation algorithm to eliminate the redundant iterations of the traditional scheme, while ensuring accuracy and robustness. Based on the feature that accurately shifted ($\pm$) 1-order spectrums have the
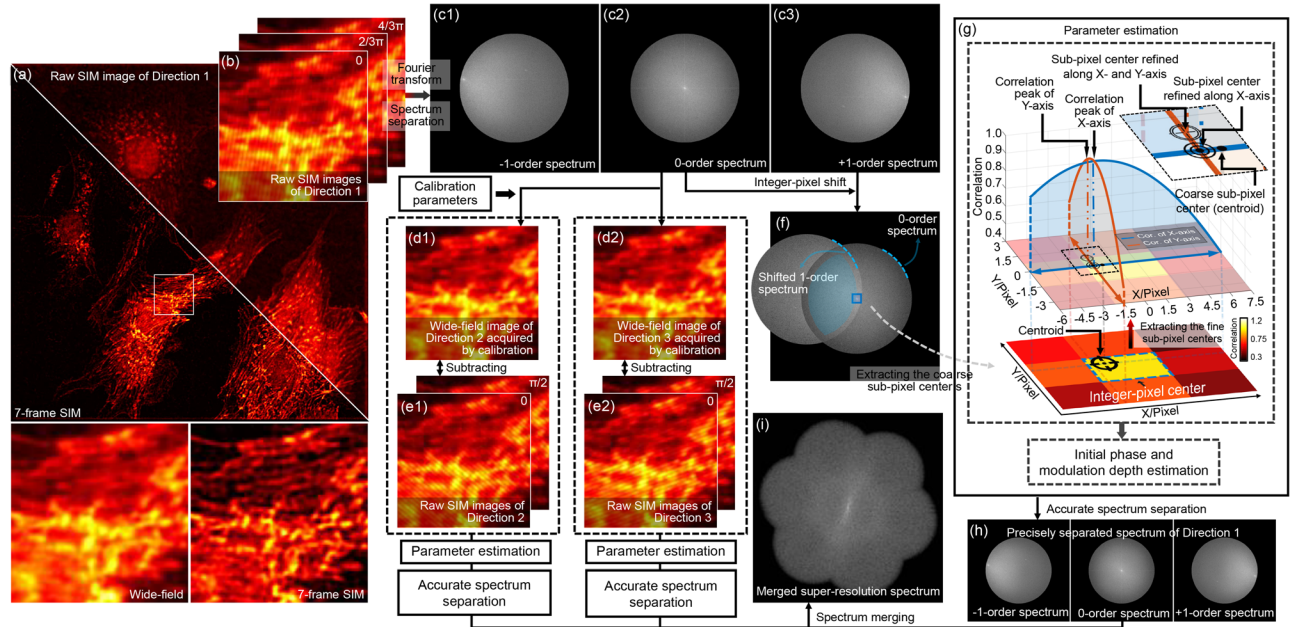
FIG. 1. Flowchart of the seven-frame SIM reconstruction algorithm combined with pixel-wise fluorescence pre-calibration. (a) Wide-field image in the first illumination direction and super-resolution image. (b) Raw SIM images in the first direction from the white boxed regions in (a). (c) Initially separated spectrums in the first illumination direction. (d) Wide-field images acquired by calibration in the second and third directions. Raw SIM images in the second and third directions. (f) The first-order spectrums of the first illumination direction shifted by integer pixels. (g) Coarse-to-fine accelerated correlation-based parameter estimation. (h) Accurately separated spectrums in the first illumination direction. (i) Merged spectrums.

maximum correlation with the zero-order spectrums, locating such a maximum correlation value is the key to obtaining the wave vector. We first calculate the correlation distribution of the one-order spectrums shifted in a specific small range $\mathbf{p}_s$ including nine whole-pixel positions $\mathbf{p}_{s,x \, or \, y} = 0, \pm 1$ and four sub-pixel positions $\mathbf{p}_{s,x \, or \, y} = \pm 0.5$, where the subscripts x and y represent the horizontal and vertical components, respectively. For simplicity, the direction parameter n is omitted in the following with the 0-order component, and the centroid coordinate $\mathbf{p}_c$ of these correlation values is obtained as follows [Figs. 1(f) and 1(g)]:

$$\mathbf{p}_c = \frac{\sum_{\mathbf{p}_s} Cor(\mathbf{p}_s)\mathbf{p}_s}{\sum_{\mathbf{p}_s} Cor(\mathbf{p}_s)}, \tag{4}$$

$$Cor(\mathbf{p}_s) = \frac{\sum_{\mathbf{k}} m\tilde{S}_0^*(\mathbf{k})\tilde{S}_{\pm 1}(\mathbf{k} \mp \mathbf{p}_{sub} \pm \mathbf{p}_s) \exp(\pm i\varphi^0)}{\sum_{\mathbf{k}} |\tilde{S}_0(\mathbf{k})|^2}, \tag{5}$$

where Cor denotes the correlation function, $*$ is the conjugate, and $\mathbf{P}_{sub}$ is the sub-pixel part of the wave vector. Note that before the above-mentioned step, all spectrum components have been deconvoluted, and the one-order spectrums have been shifted by integer pixels to relatively exact positions (the wave vector $\mathbf{p}$ can be divided into integer-pixel $\mathbf{p}_{int}$ and sub-pixel parts $\mathbf{p}_{sub}$). The acquired centroid is a coarse version of $\mathbf{p}_{sub}$. Starting from $\mathbf{p}_c$, the one-order spectrum is shifted horizontally in a small step and then the correlation between it and the zero-order component is calculated to locate the correlation peak

$$\hat{\mathbf{p}}_{sub,x} = \arg\max_{\mathbf{p}_s'} Cor(\mathbf{p}_s'), \tag{6}$$

$$\mathbf{p}_{s,y}' = \mathbf{p}_{c,y}, \quad \mathbf{p}_{s,x}' \in [-0.5 + \mathbf{p}_{c,x}, \, 0.5 + \mathbf{p}_{c,x}], \tag{7}$$

where $\mathbf{p}_s'$ represents the shift range, arg max is the operation to search for the maximum value, and $\hat{\mathbf{p}}_{sub,x}$ is the position of the found correlation peak. Then, starting from $\mathbf{p}_{sub,x}'$, the same operation is performed along the following vertical range to obtain the sub-pixel part $\hat{\mathbf{p}}_{sub}$ of the wave vector [Fig. 1(g)]:

$$\mathbf{p}_{s,y}' \in [-0.5 + \hat{\mathbf{p}}_{sub,y}, \, 0.5 + \hat{\mathbf{p}}_{sub,y}], \quad \mathbf{p}_{s,x}' = \hat{\mathbf{p}}_{sub,x}. \tag{8}$$

By performing a fast sub-pixel initial value search through few correlation operations, followed by gradient descent along only two one-dimensional lines, the efficiency of parameter estimation is more than four times that of conventional COR with multiple iterative gradient descent in progressively finer steps within a two-dimensional region, while accuracy and stability are guaranteed due to the retention of correlation operations robust to noise. When shifting the one-order spectrums to the correct position by the estimated sub-pixel wave vector, the initial phase and modulation depth can be obtained by complex linear regression

$$\varphi^0 = angle \frac{\sum_k m\tilde{S}_0^*(k)\tilde{S}_{\pm 1}(k) \exp(\pm i\varphi_n^0)}{\sum_k |\tilde{S}_0(k)|^2}, \tag{9}$$

$$m = \left| \frac{\sum_k m\tilde{S}_0^*(k)\tilde{S}_{\pm 1}(k) \exp(\pm i\varphi_n^0)}{\sum_k |\tilde{S}_0(k)|^2} \right|, \tag{10}$$

where $angle()$ represents the function that returns the phase. With these illumination parameters, all spectrum components can be
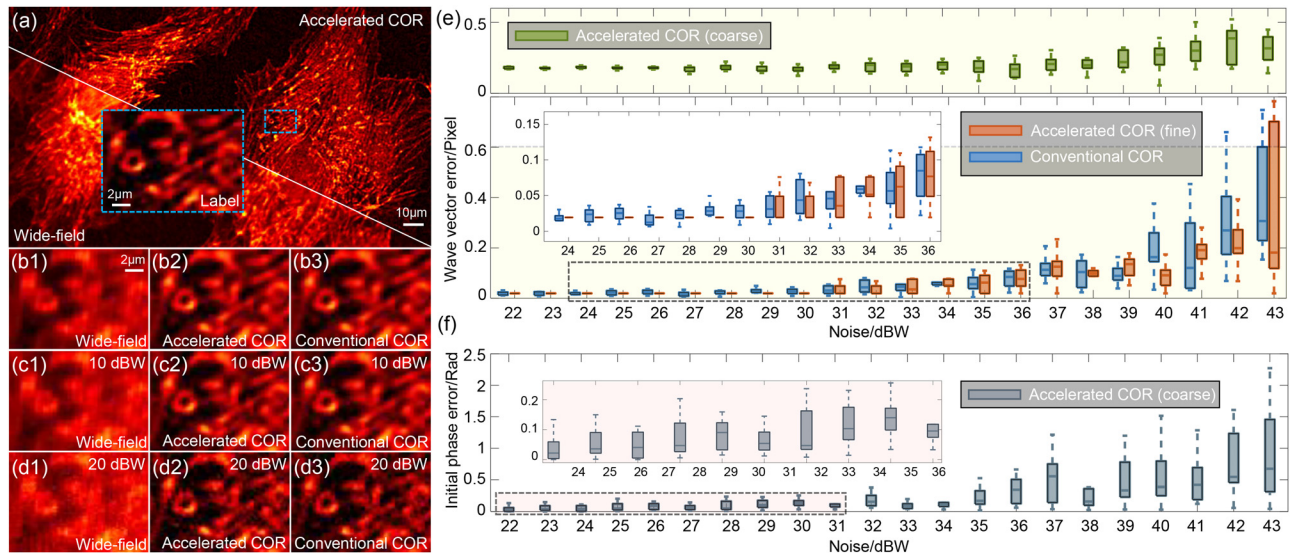
FIG. 2. Simulation comparison of parameter estimation for conventional COR and accelerated COR at different SNRs. (a) Wide-field and super-resolution images. (b)–(d) Magnified images from the blue boxed regions in (a) obtained by different methods at different SNR (e) Wave vector errors estimated by different methods at different SNRs. (f) Initial phase errors estimated by accelerated COR at different SNRs.

precisely reorganized and then super-resolution image can be acquired by Wiener filter, as shown in Figs. 1(h) and 1(i) [Note S2 of the supplementary material].

Actually, in addition to the experimental parameters, the out-of-focus background caused by sample scattering is also one of the main factors affecting the quality of SIM reconstruction, since SIM is essentially a wide-field microscopy technique. In the Fourier frequency domain, the defocus is mixed with the low-frequency information of the sample, which will also affect the separation of the one-order spectrums originally shifted to the zero-order spectrum position. Before image reconstruction, therefore, we preprocess the raw images and directly remove the unreliable backgrounds associated with low SNRs through the spatial distribution of the modulation, based on the fact
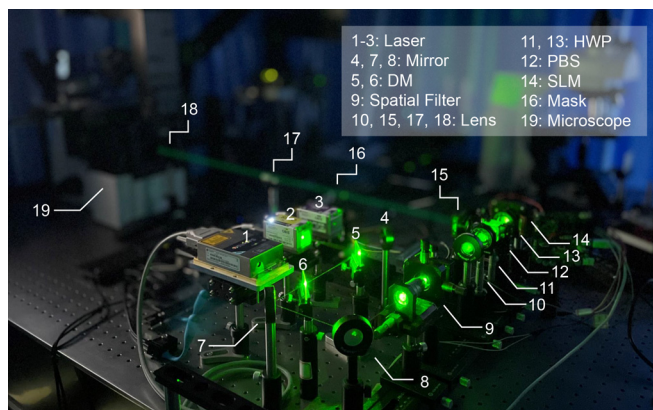

FIG. 3. The constructed interferometric SIM microscope based on Olympus IX73. DM: dichroic mirror, HWP: half-wave plate, PBS: polarization beam splitter, SLM: spatial light modulator.
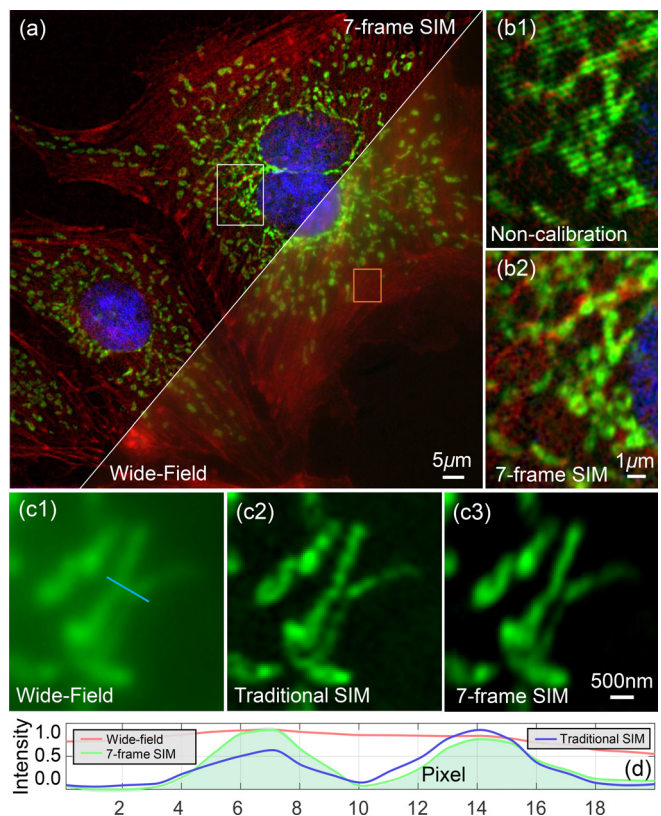

FIG. 4. Comparative experiments on super-resolution results of a BPAE cell sample. (a) Wide-field and super-resolution images. (b) and (c) Magnified images from the white and yellow boxed regions in (a) obtained by different methods. (d) Intensity profiles along light blue line in (c).

that only fluorescence signals in the imaging focal plane are sharp while those from other planes are blurred. Specifically, regions where the modulation is less than a certain threshold are considered out-of-focus backgrounds or regions with low SNRs and are spatially removed, which somewhat mitigates the effects of defocusing on spectrum separation (a detailed spatial filtration process is provided in Note S3 of the supplementary material).

We designed a series of simulations to prove the effectiveness of the proposed accelerated correlation-enabled parameter estimation. A high-resolution image of bovine pulmonary artery endothelial (BPAE) cells was used to generate the raw SIM images captured under a 40×0.6 NA objective and Gaussian noise of different powers was added manually. Figures 2(a)–2(d) show the super-resolution images acquired by conventional COR and accelerated COR at different noise powers, from which it can be seen that our approach achieves visually similar high-quality reconstruction results as conventional COR. The quantitative comparison data between our method and conventional COR at a wider range of SNRs is provided in Figs. 2(e) and 2(f). At typical noise levels, wave vector estimation with an accuracy of about 0.1 pixel is achieved by fast sub-pixel initial value search. Further refinement reaches an accuracy (less than 0.05 pixel) comparable to conventional COR [Fig. 2(e)] and the resulting initial phase accuracy of less than 0.1 rad [Fig. 2(f)]. Even at very low SNRs, our approach is only slightly inferior to conventional COR. In terms of speed, using a computer (AMD Ryzen 7 4800H CPU, NVIDIA GeForce RTX 2060) to process images with a resolution of 1024×1024 with MATLAB R2016a, it took 16.8892 ± 0.1569 s for conventional COR, but only 3.7763 ± 0.0339 s for our method. Simulation results demonstrate that our method has an optimal combination of accuracy, efficiency, and robustness.

We also verified the superiority of the proposed seven-SIM reconstruction algorithm through experiments. An interferometric SIM microscope based on Olympus IX73 equipped with a $60 \times /1.42$ NA objective len was constructed (see Note S4 of the supplementary material for details), as shown in Fig. 3. First, we measured a fixed thin BPAE sample (purchased from Thermo Fisher, and the nucleus, mitochondria, and actin are labeled by DAPI (4',6-diamidino-2-phenylindole) MitoTracker Red[TM] CMXRos, and Alexa Fluor[TM], respectively). The reconstruction results of different methods are shown in Fig. 4. As mentioned above, the fluorescence imbalance in different illumination directions leads to inaccurate spectrum separation, generating reconstruction artifacts [Fig. 4(b1)], while these are well removed after calibration [Fig. 4(b2)]. Compared with the conventional nine-frame SIM reconstruction using COR-based parameter estimation, the proposed seven-frame SIM algorithm with accelerated COR also yields high-quality super-resolution results [Fig. 4(c)]. Further analysis of the normalized fluorescence intensities of the super-resolution images reconstructed by different methods indicates that our approach has comparable resolution enhancement to the conventional method with a slight contrast improvement [Fig. 4(d)]. Finally, we imaged a home-made thick CV-1 in Origin Simian-7 (COS-7) cell sample (the nucleus, mitochondria, and actin are labeled by DAPI, Alexa Fluor 568, and MitoTracker Green FM, respectively) to verify the robustness of our approach at low SNR. As can be seen from the wide-field image in Fig. 5, the out-of-focus due to sample scattering severely affects the imaging quality. Similarly, no significant artifacts appear in the super-resolution image acquired by the proposed seven-frame reconstruction approach [Fig. 5(b)]. Moreover, thanks to the
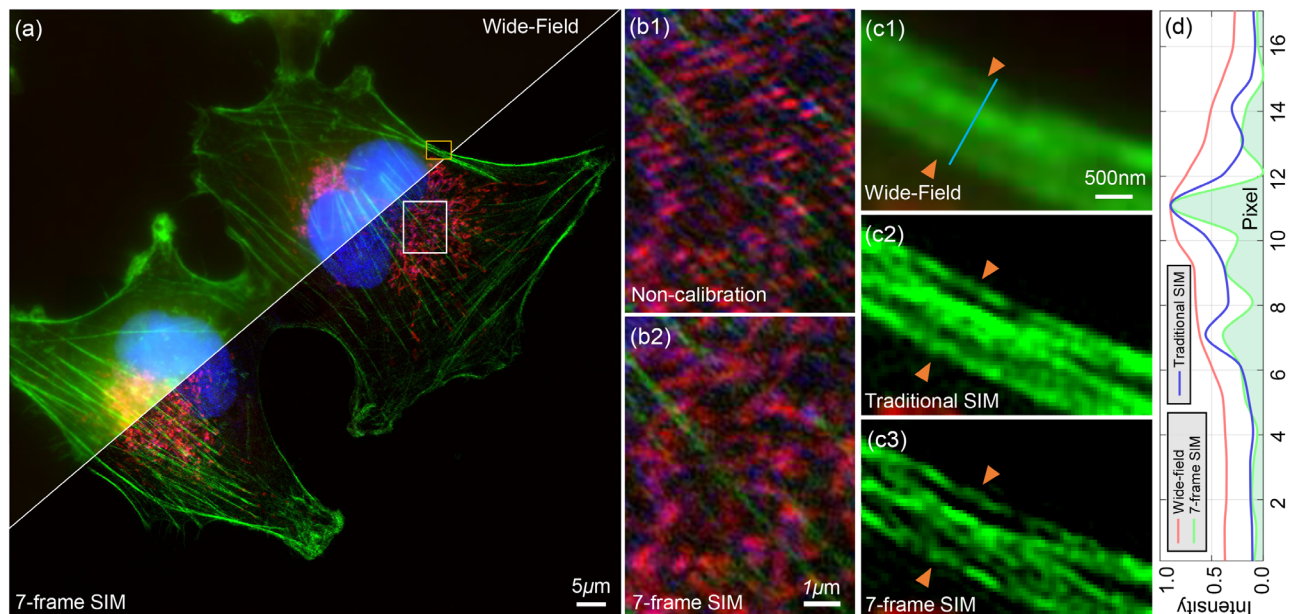

FIG. 5. Comparative experiments on super-resolution results of a thick COS-7 cell sample. (a) Wide-field and super-resolution images. (b) and (c) Magnified images from the yellow and white boxed regions in (a) obtained by different methods. (d) Intensity profiles along light blue line in (c).

preprocessing of the defocus filtering, the quality of the reconstruction result obtained by our method is superior to that of the conventional method, and for actin in COS-7 cells, our method acquires the best resolution and contrast [Figs. 5(c) and 5(d)].

To sum up, we presented a seven-frame SIM reconstruction algorithm with accelerated correlation-enabled estimation illumination. Unlike iterative frame-reduced strategies that are sensitive to illumination parameters, we perform frame reduction exploration based on the practical phase-shifting-enabled spectrum demodulation of the conventional SIM reconstruction algorithm, thus ensuring the practicality in practical fluorescence imaging. For parameter estimation, we optimize the iterative COR algorithm in terms of speed for the first time, redesigning its algorithmic framework and implementing the similarly stable and high-accuracy sub-pixel optimization, to ensure robustness to low SNRs. The proposed algorithm achieves high-quality super-resolution reconstruction in complex experimental environments with fewer raw images and faster processing speed (4.5 times faster than conventional COR), which contributes to the capability of SIM to achieve faster and longer-time live-cell observations.

See the supplementary material for more details of principles and equipments.

AUTHOR DECLARATIONS
Conflict of Interest

The authors have no conflicts to disclose.

Author Contributions

Jiaming Qian and Yu Cao contributed equally to this work.

Jiaming Qian: Conceptualization (equal); Data curation (lead); Validation (lead); Visualization (lead); Writing – original draft (lead); Writing – review & editing (lead). **Yu Cao:** Data curation (equal); Validation (equal); Writing – original draft (equal). **Kailong Xu:** Software (equal); Validation (equal). **Ying Bi:** Validation (equal); Writing – original draft (equal). **Weiyi Xia:** Visualization (equal); Writing – original draft (equal). **Qian Chen:** Conceptualization (equal); Funding acquisition (equal); Writing – review & editing (equal). **Chao Zuo:** Conceptualization (equal); Funding acquisition (equal); Supervision (equal); Writing – review & editing (equal).

DATA AVAILABILITY

The data that support the findings of this study are available from the corresponding author upon reasonable request.

REFERENCES

[1]E. Abbe, "Beiträge zur theorie des mikroskops und der mikroskopischen wahrnehmung," Arch. Mikrosk. Anat. **9**, 413–468 (1873).

[2]E. Betzig, G. H. Patterson, R. Sougrat, O. W. Lindwasser, S. Olenych, J. S. Bonifacino, M. W. Davidson, J. Lippincott-Schwartz, and H. F. Hess, "Imaging intracellular fluorescent proteins at nanometer resolution," Science **313**, 1642–1645 (2006).

[3]M. J. Rust, M. Bates, and X. Zhuang, "Sub-diffraction-limit imaging by stochastic optical reconstruction microscopy (STORM)," Nat. Methods **3**, 793–796 (2006).

[4]S. W. Hell and J. Wichmann, "Breaking the diffraction resolution limit by stimulated emission: Stimulated-emission-depletion fluorescence microscopy," Opt. Lett. **19**, 780–782 (1994).

[5]R. Heintzmann and C. G. Cremer, "Laterally modulated excitation microscopy: Improvement of resolution by using a diffraction grating," in *Optical Biopsies and Microscopic Techniques III* (SPIE, 1999), Vol. 3568, pp. 185–196.

[6]M. G. Gustafsson, "Surpassing the lateral resolution limit by a factor of two using structured illumination microscopy," J. Microsc. **198**, 82–87 (2000).

[7]M. G. Gustafsson, "Nonlinear structured-illumination microscopy: Wide-field fluorescence imaging with theoretically unlimited resolution," Proc. Natl. Acad. Sci. **102**, 13081–13086 (2005).

[8]P. Kner, B. B. Chhun, E. R. Griffis, L. Winoto, and M. G. Gustafsson, "Super-resolution video microscopy of live cells by structured illumination," Nat. Methods **6**, 339–342 (2009).

[9]L. Shao, P. Kner, E. H. Rego, and M. G. Gustafsson, "Super-resolution 3D microscopy of live whole cells using structured illumination," Nat. Methods **8**, 1044–1046 (2011).

[10]L. Schermelleh, R. Heintzmann, and H. Leonhardt, "A guide to super-resolution fluorescence microscopy," J. Cell Biol. **190**, 165–175 (2010).

[11]J. Demmerle, C. Innocent, A. J. North, G. Ball, M. Müller, E. Miron, A. Matsuda, I. M. Dobbie, Y. Markaki, and L. Schermelleh, "Strategic and practical guidelines for successful structured illumination microscopy," Nat. Protoc. **12**, 988–1010 (2017).

[12]F. Orieux, E. Sepulveda, V. Loriette, B. Dubertret, and J.-C. Olivo-Marin, "Bayesian estimation for optimized structured illumination microscopy," IEEE Trans. Image Process. **21**, 601–614 (2012).

[13]F. Ströhl and C. F. Kaminski, "Speed limits of structured illumination microscopy," Opt. Lett. **42**, 2511–2514 (2017).

[14]S. Dong, J. Liao, K. Guo, L. Bian, J. Suo, and G. Zheng, "Resolution doubling with a reduced number of image acquisitions," Biomed. Opt. Express **6**, 2946–2952 (2015).

[15]A. Lal, C. Shan, K. Zhao, W. Liu, X. Huang, W. Zong, L. Chen, and P. Xi, "A frequency domain SIM reconstruction algorithm using reduced number of images," IEEE Trans. Image Process. **27**, 4555–4570 (2018).

[16]L. Jin, B. Liu, F. Zhao, S. Hahn, B. Dong, R. Song, T. C. Elston, Y. Xu, and K. M. Hahn, "Deep learning enables structured illumination microscopy with low light levels and enhanced speed," Nat. Commun. **11**, 1934 (2020).

[17]C. Ling, C. Zhang, M. Wang, F. Meng, L. Du, and X. Yuan, "Fast structured illumination microscopy via deep learning," Photonics Res. **8**, 1350–1359 (2020).

[18]C. Zuo, J. Qian, S. Feng, W. Yin, Y. Li, P. Fan, J. Han, K. Qian, and Q. Chen, "Deep learning in optical metrology: A review," Light **11**, 39 (2022).

[19]X. Huang, J. Fan, L. Li, H. Liu, R. Wu, Y. Wu, L. Wei, H. Mao, A. Lal, P. Xi *et al.*, "Fast, long-term, super-resolution imaging with Hessian structured illumination microscopy," Nat. Biotechnol. **36**, 451–459 (2018).

[20]G. Wen, S. Li, L. Wang, X. Chen, Z. Sun, Y. Liang, X. Jin, Y. Xing, Y. Jiu, Y. Tang *et al.*, "High-fidelity structured illumination microscopy by point-spread-function engineering," Light **10**, 70 (2021).

[21]S. A. Shroff, J. R. Fienup, and D. R. Williams, "Phase-shift estimation in sinusoidally illuminated images for lateral superresolution," J. Opt. Soc. Am. A **26**, 413–424 (2009).

[22]K. Wicker, "Non-iterative determination of pattern phase in structured illumination microscopy using auto-correlations in Fourier space," Opt. Express **21**, 24692–24701 (2013).

[23]X. Zhou, M. Lei, D. Dan, B. Yao, Y. Yang, J. Qian, G. Chen, and P. R. Bianco, "Image recombination transform algorithm for superresolution structured illumination microscopy," J. Biomed. Opt. **21**, 096009 (2016).

[24]M. G. Gustafsson, L. Shao, P. M. Carlton, C. R. Wang, I. N. Golubovskaya, W. Z. Cande, D. A. Agard, and J. W. Sedat, "Three-dimensional resolution doubling in wide-field fluorescence microscopy by structured illumination," Biophys. J. **94**, 4957–4970 (2008).

[25]K. Wicker, O. Mandula, G. Best, R. Fiolka, and R. Heintzmann, "Phase ptimization for structured illumination microscopy," Opt. Express **21**, 2032–2049 (2013).